Wave breaking for Boussinesq-type models using a turbulence kinetic energy model

Maria Kazolea, Mario Ricchiuto

Wave breaking for Boussinesq-type models using a turbulence kinetic energy model

M. Kazolea, M. Ricchiuto*

RESEARCH REPORT
N° 8781
March 2016
Project-Team CARDAMOM

ISSN 0249-6399 ISRN INRIA/RR--8781--FR+ENG

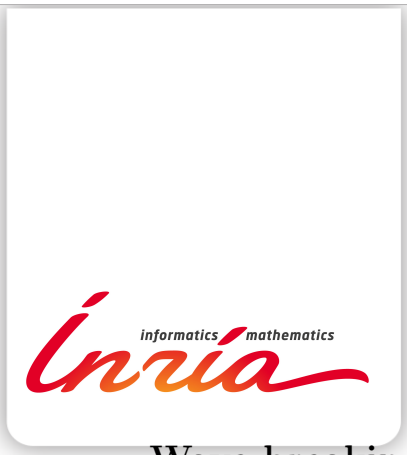

Wave breaking for Boussinesq-type models using a turbulence kinetic energy model

M. Kazolea*, M. Ricchiuto*

Project-Team CARDAMOM

Research Report n° 8781 — March 2016 — 18 pages

Abstract: This work aims at providing a simple and improved description of wave breaking in the framework of Boussinesq type modelling. In particular, we evaluate the coupling of both a weakly and a fully non-linear Boussinesq system with a turbulence model. We reformulate an evolution model for the turbulent kinetic energy, initially proposed by Nwogu, and evaluate its capabilities to provide sufficient dissipation in breaking regions. We also compare this dissipationto the one introduced by the numerical discretization.

Key-words: Boussinesq equations, Wave breaking, Finite Volumes, eddy viscosity, turbulence model

* Inria BSO, Team CARDAMOM

RESEARCH CENTRE
BORDEAUX – SUD-OUEST

351, Cours de la Libération
Bâtiment A 29
33405 Talence Cedex

Wave breaking for Boussinesq-type models using a turbulence kinetic energy model

Résumé : Ce travail vise à une description améliorée de vagues déferlantes dans le cadre d'une modélisation type Boussinesq. Nous ́valuons le couplage entre des modèles type weakly et fully non-lienar avec un modèle de turbulence. Nous reformulons un modèle d'evolutions pour l'énergie cinétique turbulente initialement proposé par Nwogu, et nous évaluons ses capacités à fournir une dissipation suffisante dans les régions déferlantes. Nous comparons aussi cette dissipation avec celle du schéma numérique utilisé pour approximer les équations.

Mots-clés : Boussinesq equations, Wave breaking, Finite Volumes, eddy viscosity, turbulence model

Contents

1 Introduction

The last decades many numerical models, based on Boussinesq-type (BT) equations, that simulate wave propagation from intermediate depths to shallow water have been developed. Further more several authors have extended BT models to simulate wave breaking in the surf zone. An extensive review of the different wave breaking techniques developed until now can be found in [2, 10]. In this work we use two sets of BT equations the one of Nwogu [15] and the Green-Nagdhi equations and we employ a one-equation turbulence model to describe the temporal and spatial evolution of the turbulent kinetic energy produced by wave breaking. The rate of production of turbulent kinetic energy is assumed to be proportional to the vertical gradient of the horizontal water particle velocity at the wave crest.

In the second section the Boussinesqs formulation along with the turbulent model are presented. In section 3 both numerical models are briefly presented, along with the discretization of the dispersive terms, and the time iteration procedure. The bathymetry source term is discretized as to provide a well-balanced scheme, also in the presence of wet/dry fronts which are properly handled in the numerical model. In section 4 some preliminary results of standard test cases, involving wave breaking, are presented.

2 Governing Equations

2.1 Weakly nonlinear-Weakly dispersive

Nwogu [15] derived a system of equations using the velocity u_a at an arbitrary distance from a still water level z_a as the velocity variable, instead of the commonly used depth-averaged velocity. An optimum value of $z_a = 0.531d$ was used,where d denotes the still water depth, so that the dispersion properties of the system most closely approximate those defined by linear wave theory, making the equations applicable to a wider range of water depths. The equations of Nwogu consist of a continuity and a momentum equation. Following [17] we can write the equations in a vector form:

$$\mathbf{U}_t + \mathbf{F}(\mathbf{U}^*)_x = \mathbf{S}(\mathbf{U}), \tag{1}$$

where $\mathbf{U}$ is the vector of the new variables, $\mathbf{U}^*$ is the vector of the conserved variables, $\mathbf{F}$ is the flux vector and $\mathbf{S}$ is the source term,

$$\mathbf{U} = \begin{bmatrix} H \\ P^* \end{bmatrix}, \quad \mathbf{F}(\mathbf{U}) = \begin{bmatrix} Hu \\ Hu^2 + \frac{1}{2}gH^2 \end{bmatrix}.$$

$H = d+\eta$ is the total water depth, η the free surface elevation and $u_a \equiv u$ is the horizontal flow velocity.

$$P^* = Hu + Hz_a\left(\frac{z_a}{2}u_{xx} + (du)_{xx}\right) \tag{2}$$

is the velocity function and contains all time-derivatives in the momentum equation and a part of the dispersion terms. The subscripts x and t denote partial derivatives with respect to space and time and g is the gravitational acceleration. The source term $\mathbf{S}(\mathbf{U}) = \mathbf{S_b} + \mathbf{S_f} + \mathbf{S_d}$ models the effects of the shape of the topography, friction and a part of the dispersion terms. By denoting with b the bed topography elevation, the geometrical source term is given as $\mathbf{S_b} = [0 \ \ -gHb_x]^T$, the source term component $\mathbf{S_f}$ includes the bed friction stresses, given as $\mathbf{S_f} = [0 \ \ -gHS_f]$ with $S_f = \frac{n_m^2 u||u||}{H^{-4/3}}$ and $\mathbf{S_d} = [-\psi_C \ \ -u\psi_C + \psi_M - F_{br}]$ contains the dispersion terms.

$$\psi_M = H_t z_a\left(\frac{z_a}{2}u_{xx} + (du)_{xx}\right), \quad \psi_C = \left[\left(\frac{z_a^2}{2} - \frac{d^2}{6}\right)du_{xx} + \left(z_a + \frac{d}{2}\right)d(du)_{xx}\right]_x. \tag{3}$$

R_b represents the parametrization of wave-breaking characteristics.

2.2 Fully nonlinear-weakly dispersive

An other set of equation used in this work are the Green-Nagdhi (GN) partial differential equations. They are widely used for the simulation of fully nonlinear, weakly dispersive free surface waves. The range of validity of the model may vary as much as far for the nonlinearity parameter (ϵ) is concerend but it requires that the shallowness parameter (μ) to be small (less than one). In this work we use the numerical model developed in [7], based on the system of equations reading

$$\begin{aligned} h_t + (hu)_x &= 0 \\ (I + \alpha\mathcal{T})\left[(hu)_t + (hu^2)_x + g\frac{\alpha - 1}{\alpha}h\eta_x\right] + \frac{g}{\alpha}h\eta_x + h\mathcal{Q}(u) &= 0 \end{aligned} \tag{4}$$

where the non-linear operator $\mathcal{Q}(\cdot)$ is defined by

$$\mathcal{Q}(\cdot) = 2hh_x(\cdot)_x^2 + \frac{4}{3}h^2(\cdot)_x(\cdot)_{xx} + b_x h(\cdot)_x^2 + b_{xx}h(\cdot)(\cdot)_x + \left[b_{xx}h_x + \frac{1}{2}hb_{xxx} + b_x b_{xx}\right](\cdot)^2 \tag{5}$$

The operator $\mathcal{T}(\cdot)$ plays a key role, as its inversion is necessary to be able to obtain evolution equations for the physical variables. For this reason, following [**?**] it is important to stress that $\mathcal{T}(\cdot)$ can be written in a compact form involving two operators $S_1(\cdot)$ and $S_2(\cdot)$ and their adjoints $S_1^*(\cdot)$ and $S_2^*(\cdot)$, namely

$$\mathcal{T}(\cdot) = S_1^*\left(hS_1\left(\frac{(\cdot)}{h}\right)\right) + S_2^*\left(hS_2\left(\frac{(\cdot)}{h}\right)\right) \tag{6}$$

where in one space dimension we have

$$S_1(\cdot) = \frac{h}{\sqrt{3}}(\cdot)_x - \frac{\sqrt{3}}{2}b_x(\cdot), \qquad S_2(\cdot) = \frac{1}{2}b_x(\cdot) \tag{7}$$

The above system, given an initial condition can be now be solved in two independent steps. An elliptic step solving for the non-hydrostatic term ϕ and an hyberbolic step evolving the flow variables.

2.3 Turbulence model

The shallow water steepness is the primary cause of breaking for waves on a beach. As the wave amplitude increases and reaches a critical level wave crest steepen, the front of the wave becomes vertical and then the crest of the wave overturns. At this point physical models like Boussinesq equations are unable to describe the physical procedure and a wave breaking model is necessary. One way to parametrize the effect of wave breaking is by the addition of an eddy viscosity term in the momentum equation. Nwogu [16] used a dissipative term of the form $\mathbf{F}_{br} = -v_t \nabla(\nabla \cdot \mathbf{u})$ where v_t is the turbulent eddy viscosity. As pointed out by Kennedy [11] and Roeber [17] its important o dissipate energy but also conserve the momentum to accurately capture details of the mean flow field associated with breaking waves. So a modified form is used:

$$\mathbf{F}_{br} = -\nabla(v_t \nabla \cdot H\mathbf{u})$$

which for the 1D case is reduced to $\mathbf{F}_{br} = -\left(v_t (Hu)_x\right)_x$.

The eddy viscosity is determined from the amount of the turbulent kinetic energy produced by the wave breaking and a turbulent length scale ℓ_t by: $v_t = -\sqrt{k}\ell_t$. Following the work of [16] the turbulent kinetic energy is determined from a semi-empirical transport equation with a source term for turbulent kinetic energy production by wave breaking:

$$k_t + u_s k_x = \sigma v_t k_{xx} + B \frac{\ell_t^2}{\sqrt{C_D}} \left[u_z^2\right]_{z=\eta}^{3/2} \tag{8}$$

The surface velocity and the velocity gradient $u_z|_\eta$ for Nwogu's equations, can be computed using the horizontal velocity over depth [15] so

$$u_s = u + (z_a - \eta)(du)_{xx} + \frac{1}{2}(z_a^2 - \eta^2) u_{xx} \tag{9}$$

and

$$u_z = -z u_{xx} - (du)_{xx}. \tag{10}$$

For the GN equations the surface velocity and the velocity gradient should also be extracted. Expanding the horizondal velocities as Taylor series about the seabed ($z = -h$) and after substitution of the vertical velocity and integration of the irrotetionality condition over depth [15] we get:

$$u(z) = u_b + \mu^2 \left(\frac{d^2}{2} - \frac{z^2}{2}\right)(u_b)_{xx} - \mu^2 (d+z)(h u_b)_{xx} + O(\mu^4) \tag{11}$$

where $u_b = u(x, -d, t)$ is the velocity at the bottom. Integrating equation (11) over the depth, keeping all the terms up to $O(\mu^4)$ and after some calculus the velocity $u(z)$ in terms of the mean velocity value can be expressed as:

$$u(z) = \bar{u} - \left(-\frac{d^2}{6} - \frac{\eta^2}{6} + \frac{\eta d}{6} + \frac{z^2}{2}\right)\bar{u}_{xx} - \left(\frac{d-\eta}{2} + z\right)(d\bar{u})_x x \tag{12}$$

so evaluating the above relation at the surface level and dropping the bar from the mean velocity we get:

$$u_s = u - \frac{1}{6}\left(-d^2 + 2\eta^2 + \eta d\right) u_{xx} - \frac{1}{2}(d+\eta)(du)_{xx}. \tag{13}$$

By differentiating (11), the velocity gradient reads as:

$$u_z = -z u_{xx} - (du)_{xx} \tag{14}$$

The first term on the right hand side of equation (8) represent the horizontal diffusion of turbulent kinetic energy and the second term represent the production of turbulent kinetic energy due to wave breaking. The parameter B is introduced to ensure that turbulence is produced after waves break. In [16] turbulence is produced only when horizontal velocity at the wave crest (u_s) exceeds the phase velocity of the waves.

In this work the criteria used to characterize wave breaking are those presented in [10] and have been found more robust. More precisely:

- the surface variation criterion: $|\eta_t| \geq \gamma\sqrt{gh}$ with the value of $\gamma \in [0.3, \quad 0.65]$ depending on the physical configuration and
- the local slope angle criterion: $||\nabla\eta|| \geq tan(\varphi_c)$, where φ_c is the critical front face angle at the initiation of breaking.

If one of the above criteria is satisfied $B = 1$ else $B = 0$. The first criterion flags for breaking when is positive, as breaking starts on the front face of the wave and has the advantage that can be easily calculated during the running of the model. The second criterion acts complementary to the first one as to better detect stationary or slow-moving hydraulic jumps that might otherwise not be detected from the first criterion [17, 10]

The last term on the right hand side of equation (8) represents the dissipation of turbulent kinetic energy into heat. C_D and σ are empirical constants and here have been chosen as 0.08 and 0.2 even though different values can be chosen producing similar results. The turbulent length scale ℓ_t remains the only free parameter. Following [16, 4] ℓ_t is chosen to be on the order of the wave height.

2.4 Energy equations

Generally speaking the different wave breaking techniques in Boussinesq-type modeling, either by switching of the dispersive terms or by considering the inclusion of an extra term in the momentum equation, they try to mimic the dissipation of energy when wave breaking is likely to occur. Up to the authors knowledge the only work which considers the topic of the energy dissipation of BT models is the one of Briganti et al. [1]. According to [1] the energy dissipation is usually the sum of three main contributions: 1. the theoretical contribution coming from the breaking-type terms, 2. the intrinsic numerical contribution coming from the numerical scheme in use and 3. the extrinsic numerical contribution coming from any stabilizing mechanism ad-hoc introduced to get stable solutions (e.g. filters which are used to get-rid of high-frequency osculations).

As to study the energy dissipation produced during breaking, we have to define the energy variation laws for the weakly non-linear weakly dispersive model and for the highly non-linear highly dispersive model. For the first set of equation we use the energy associated to the Boussinesq system assuming small topography variations [12]:

$$E_B = \sum_i \left[\frac{1}{2}\left(Hu^2 + g\eta^2\right) + \frac{1}{2}\left(\frac{d^2}{3}u_x^2 - d^2 u_x b_x - \frac{3}{4}d b_x^2 + \frac{1}{4}b_x^2 u^2 \right) \right] \tag{15}$$

The intrinsic numerical contribution coming from the numerical scheme used (see also section 3) can be computed as:

$$E_F = E_{i+1/2} = \left(\frac{V_i + V_{i+1}}{2} \right)^T |A|_{i+1/2} \left(U_R - U_L\right)_{i+1/2} \tag{16}$$

where

$$V_i = (g\eta - \frac{u^2}{2},\ u)_i^T, \quad U_i = (H,\ Hu)_i^T$$

and $A_{i+1/2}$ is the Roe average Jacobian Matrix, while the one coming from the breaking terms can read as:

$$E_{tur} = u_i(v_t(Hu)_x)_x. \tag{17}$$

For the GN equations and following [6] we can write the energy equation as:

$$E_{GN} = \left[\frac{1}{2}\left(Hu^2 + g\eta^2\right) + \frac{1}{2}\left(\frac{d^2}{3}u_x^2 - d^2u_xb_x - \frac{3}{4}db_x^2 + \frac{1}{4}b_x^2u^2\right)\right] \tag{18}$$

3 Numerical schemes

The numerical scheme used to solve the equations of Nwogu is fourth order in space and in time. It is a hybrid finite volume/finite difference scheme. We use the finite volume formulation for the discretization of the advective part of the equations and the bed source term and the finite difference formulation for the dispersive terms.

The hyperbolic part is solved with a finite volume (FV) method based on Roe's approximate Riemann solver, and with a well-balanced upwind treatment of the topography source term. High-order accuracy in the calculation of fluxes is achieved by constructing cell interface values using a fourth order Monotonic Upstream Scheme for Conservation Laws (MUSCL), prior to the application of the Riemann solve. The fourth order reconstruction is done, to the variables of total water depth H, velocity u, and bed b.

The dispersion terms contain spatial derivatives of up to third order. According to [19] a fourth order accurate treatment of the first-order derivatives is required so that the truncation errors in the numerical scheme are smaller than the dispersion terms present in the model. We discretize them using fourth order central difference approximations for first order derivatives, third order central difference approximations for third order derivatives and second order for second order derivatives.

As proposed by Wei and Kirby [19], time integration should be fourth-order accurate since first to third order spatial derivatives are included in both formulations. Here, time integration is achieved in two stages, namely the third order Adams-Basforth predictor stage and the fourth-order Adams-Moulton corrector stage.

The predictor and the corrector stages update the values of the velocity function P^* given by equation (2). The values of hu and therefore the velocities need to be extracted after, booth stages, by solving a tridiagonal system resulting from the discretizations of the spatial derivatives by using the finite difference method. In order to handle the friction terms a separate implicit formulation [3] was applied after the predictor and the corrector stages.

In order to keep the C-property in the fourth order MUSCL discretization an extra term is added to the source term discretization for maintaining the correct balance [3]. In the boundary defined by a wet/dry front a special treatment is needed. In order to identify a dry cell, a tolerance parameter is used. Reconstructed values are computed as to satisfy $\frac{\partial h}{\partial x} = -\frac{\partial b}{\partial x}$. Bed slope is redefined as to satisfy an extended $C-$property [3] and numerical fluxes at the wet/dry interface are computed assuming temporarily zero velocity. Finally the error due to possible negative depths or due to the imposed threshold are summed and added properly into the entire computational domain. More details for the discretization can be found in [9].

For the GN equations we use the numerical scheme presented in [7]. It is a hybrid strategy that involves a two step procedure. In the first step the non hydrostatic source term is recovered by inverting the elliptic coercive operator associated to the dispersive effects; in the second step the solution of the hyperbolic shallow water system with the source term , computed in the previous phase and which accounts for the non-hydrostatic effects, is retrieved. For the discretization of the two steps appropriate numerical methods are used. The standard C^0 Galerkin finite element method for the elliptic phase and a

third order Finite Volume scheme for the hyperbolic phase are used. The Finite Volume scheme, again, is of a Godunov type, uses the approximate Riemann solver of Roe along with well-balanced topography source term upwinding. High-order accuracy in the calculation of fluxes is achieved using a third order order MUSCL scheme. As before we use the Adams-Moulton time discretization for the numerical integration in time.

To numerically solve the turbulence kinetic energy equation (8) we use the finite difference technique. More precisely second order centered finite differences are used for the derivatives in space. For all breaking events the breaking term, the surface velocity and the gradient of the velocity are filtered for stability using a five-point filter before inserted into (1).

3.1 Wave generation

The internal generation of wave motion is performed following the approach of Wei. et al. [20]. The method employs a source term added to the mass equation. This source function was obtained using Fourier transform and Green's functions to solve the linearized and non-homogeneous equations of Peregrine and Nwogu. In the present model, this source function wave making method is adopted in order to let the reflected waves outgo through the wave generator freely.

To obtain a desired oscillation signal in the wave generating area, a source function $S(\mathbf{x},t)$ is added into the mass conservation equation at each time step, which is expressed as

$$S(\mathbf{x},t) = D^* \exp\left(\gamma(x-x_s)^2\right)\sin(\lambda y - \omega t) \tag{19}$$

in which

$$\gamma = \frac{5}{(\delta L/4)^2} = \frac{80}{\delta^2 L^2} \tag{20}$$

where L is the wave length, ω the wave frequency, θ the wave incident angle, $\lambda(= k_y = k\sin\theta)$ the wave number in the $y-$direction, x_s is the location of the center of the wave-making area, δ is a parameter that influences the width $W = \delta L/2$ of the wave generator area and D^* is the source function's amplitude. For a monochromatic wave, D^* is defined as

$$D^* = \frac{2\sqrt{\gamma}A_0\cos\theta\left(\omega^2 - \alpha_1 g k^4 h^3\right)}{\omega k\sqrt{\pi}\exp(-l^2/4\gamma)\left[1-\alpha(kh)^2\right]} \tag{21}$$

where h is the still water level at the wave generation region, A_0 the wave amplitude, $l(= k_x = k\cos\theta)$ the wave number in the $x-$direction, $\alpha = -0.390$ and $\alpha_1 = \alpha + 1/3$.

For irregular waves and following [8] we use the linear superposition of component waves. According to the irregular wave concept of Longuet and Higgings (1961) the water surface elevation can be described by

$$\eta(t) = \sum_{i=1}^{\inf} a_i \cos(\omega_i t + \epsilon_i)$$

where, a_i and ω_i represent the amplitude and frequency of the component wave respectively and ϵ_i denotes the initial phase of the component wave, which is distributed randomly in the range of $0-2\pi$. This means that each component wave has its deterministic amplitude and frequency. The source function now is:

$$S(\mathbf{x},t) = \exp\left(\gamma(x-x_s)^2\right)\sum_{i=1}^{M} D_i^* \sin(\lambda_i y - \omega_i t + \epsilon_i) \tag{22}$$

where the source function's amplitude is now

$$D_i^* = \frac{2\sqrt{\gamma}A_i\cos\theta_i\left(\omega_i^2 - \alpha_1 g k_i^4 h^3\right)}{\omega k_i\sqrt{\pi}\exp(-l_i^2/4\gamma)\left[1-\alpha(k_i h)^2\right]} \tag{23}$$

with $l_i = k_i \sin(\theta_i)$. For the wave making area W we use the maximum wavelength between the components.

4 Numerical results

4.1 Regular wave propagation

Hansen and Svendsen performed a number of regular wave test on plane slopes in order to study wave shoaling and breaking on a sloping beach. Waves were generated over a $0.36m$ horizontal bottom, propagated shoaled and broke over a slope of 1:32.26. One of these experiments (case 051041), producing breaker type of a spilling breaker, is recreated numerically in this work. Extensive description of the experiment can be found in [10]. The period of the incident wave is 2.0s and the wave height is 0.036m. The numerical domain $x \in [-26\ 26]$ was discretized using $\Delta x = 0.0063m$ and the CFL was 0.3. For the surface variation criterion $\gamma = 0.6$ while for the turbulence model $\ell_t = 0.036$. The

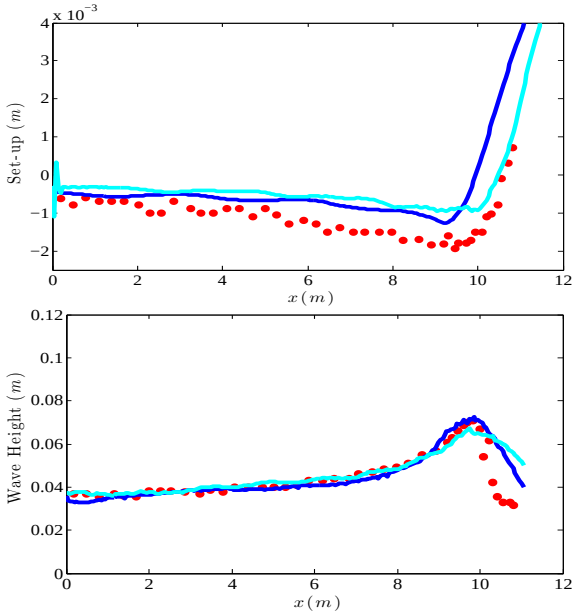

Figure 1: Computed and measured wave heights (top) and set-up (bottom). Blue line-Nwogu's equations, cyan line-GN equations.

numerical results of the model are compared to the experimental data in Fig. 1. The results show the computed and measured wave heights and MWL as the wave propagates shoal and breaks up the slope. The wave breaking formulation predict reasonably well the location of the breaking event, that happens slightly earlier compared to the experimental data. This is due to the overshoaling produced in the numerical wave, which is closely connected to the nature of the weakly nonlinear weakly dispersive BT model used here.

4.2 Solitary wave breaking over a slope

In this case we want to study propagation, breaking and run-up of a solitary wave over a planar beach with a slope 1 : 19.85. With this test case we asses the ability of our model to describe shoreline motions and wave breaking when it occurs. The incident wave height considered in this case is $A/d = 0.28$ with $d = 1$, so according to Synolakis

the wave breaks strongly both in the run-up and in the rundown phase of the motion. We consider a computational domain $x \in [-20,\ 100]$ and the computational parameters used are: $\Delta x = 0.05, CFL = 0.3$. A sponge layer is applied off-shore with length $Ls = 5m$. A Manning coefficient of $n_m = 0.01$ was used to define the glass surface roughness used in the experiments. For the surface variation breaking criterion, γ was set equal to 0.6. For the turbulence model Figure 2 compare the measured surface profiles and the numerical model's results on different dimensionless times.

Until time $t\sqrt{g/h} = 10$ the solitary propagates to the shore and the two models produce, as expected, identical results since wave breaking hasn't started yet. The experimental wave breaks around $t\sqrt{g/h} = 20$. The numerical solution for the new hybrid model is represented like a bore storing the water spilled from the breaking wave behind the front. At time $t\sqrt{g/h} = 20$ the turbulence model represents the solution as a triangular bore. Similar behavior has been observed by other researchers that use eddy viscosity models. At time $t\sqrt{g/h} = 25$ the bore collapses at the shore and the results shows good qualitative agreement. After that the wave starts to run-up. The time of maximum run-up occurs at $t\sqrt{g/h} = 45$. Up to that time the computed solution fully recovers due to the volume conservation. As the water recedes a breaking wave is created near the still water level. The numerical solution is approximated as a hydraulic jump. Even though the model is able to recognize the solution the diffusion added by the turbulence model is not enough so further research must be done concerning the treatment of hydraulic jumps.

4.3 Wave breaking over a bar

An extensive description of the test can be found in [10]. We consider here the test case with wave height $0.054m$ and $T = 2.5s$ wave period that corresponds to the water depth parameter $kh \approx 0.52$, with depth to wavelength ratio of $h/L = 0.0835$. The wave-making internal source function at $x = 0m$. The dimensions of the computational domain were set to $x \in [-10, 29m]$ with sponge layer widths is set to $L_s = 7.m$ at both ends of the computational domain. Δx set to 0.05. The CFL number used was set equal to 0.35 with the value of γ now set to 0.3 and $\ell_t = 0.2$. Four wave gauges placed at $x = 6, 12, 13$ and $14m$ respectively are examined. In the wave evolution, waves shoal along the front slope, since nonlinear effects cause the waves propagating along this slope to steepen and broke at the beginning of the bar crest. Breaking is classified as plunging. In the lee side, the back slope causes the wave train to breakup into independent waves traveling at their own speed. Even though Demirbliek and Nwogu in [5] use different wave breaking formulation for spilling and plunging wave breaking (as they declare that the turbulence model is not applicable to plunging breakers), we found out that the turbulent kinetic energy formulation combined with the physical criteria for the initiation and termination of the process can simulate reasonably well both wave breakers.

4.4 Wave breaking of bichromatic wave groups

Mase [14] performed a number of experimental test cases as to study shoaling, breaking and runup of various types of bichromatic wave trains on mild slopes. The set up of the problem can be found in [14], [18] and [13]. In this work only one wave pattern is reproduced and can be described by the following equation:

$$\eta = a_1 \cos(2\pi f_1 t) + a_1 \cos(2\pi f_2 t) \tag{24}$$

with $f_1 = 1.05 f_m$ and $f_1 = 0.95 f_m$, $a_1 = 0.15cm$ is the wave amplitude which corresponds to medium energy level and f_m denotes the mean frequency with values $f_m = 1.0, 0.6.0.3Hz$ for test cases A-C respectively. The pattern of the wave train consists of ten individual waves. The variation on mean frequency corresponds to a variation in the

wave characteristics, as f_m is reduced, the deep water wave steepness decreases and different form of wave breaking occurs. More precisely and for $f_m = 1Hz$ and $f_m = 0.6Hz$ the predominant breaker type is of a spilling breaker while for $f_m = 0.3Hz$ is of a plunging breaker. In this work we examine the case with $f_m = 0.6Hz$.

The numerical domain is $40m$. Waves are generated internally at $x = 0m$ and a sponge layer of $4m$ is placed on the offshore boundary. Grid size $\Delta x = 0.02m$ and CFL=0.3. For all the test cases the hybrid wave breaking model is used . Further more for test case B we also used the turbulance wave breaking model and the results are compared.

We have to denote that in the experiments the generation of spurious harmonics was not compensated at the generator and that there was no active absorption of reflected waves, therefore it is difficult to reproduce the laboratory conditions exactly. Furthermore, the measured frequencies and amplitudes deviated slightly from the target. Different approaches have been used as to obtain numerically the desired signal. In [13] the numerical model boundary has been placed to the first's gauge position (at the toe of the beach). The energy on the primary frequencies and their super-harmonics propagates mainly onshore while subharmonic energy will propagate offshore as well as onshore. The waves are generated internally at WG1. Tonelli et al. in [18] generated the waves internally using linear theory. They used several trials to find the best mach with the measured waves. In this work we follow [18] and we used slightly different f_m than the theoretical as to mach the experimental data at the first gauge. So, f_m used is equal to $0.61Hz$. Figure 4 compare the experimental time series of the surface elevation at the wave gauges WG8, WG10, WG12 and the time series for the vertical shoreline displacement. The two schemes are presented and compared.

4.5 Energy dissipation

As described in section 2.4 a first attempt to study the energy dissipation produced during breaking is presented here. For this reason the solitary wave breaking over a slope test case will be used (see section 4.2). Figure 4.5 shows the energy evolution during time for the Nowgu's scheme. More precisely the figure on the left depicts the intrinsic numerical contribution coming from the numerical scheme used and the one produced due to braking. The one on the right shows the the relative energy evolution using eq. (15) and the one using the energy equation form of the shallow water equations which is presented just for comparison purposes. We can observe that the total energy starts to change as the shoaling process begins while, as expected the loss of energy due to the breaking terms starts around 4. sec namely the beginning of the breaking process. We can see that the loss of energy due to the intrinsic numerical contribution coming from the numerical scheme used is insignificant compared to the one due to breaking. The next figure 4.5 depicts the same but for the GN equations. As before the energy loss deviated mostly from the one produced by the breaking terms starts at the beginning of breaking and continues until the run-up of the wave.

5 Conclusions

Two numerical schemes for numerical solving the Boussinesq-type equations of Nwogu and the GN is presented. A hybrid finite volume-finite difference technique is used for the first set of the equations while a hybrid finite volume- finite element technique is used for the GN equations . The Boussinesq-type models are extended to the surf and swash zones by coupling the mass and momentum equations with a one-equation model for the temporal and spatial evolution of the turbulent kinetic energy produced by wave breaking.

Acknowledgments

Work partially funded by the TANDEM contract, reference ANR-11-RSNR-0023-01 of the French *Programme Investissements d'Avenir*.

References

[1] Briganti, R., Musumeci, R. E., Belloti, G., Brocchini, M. & Foti, E. 2004 Boussinesq modeling of breaking waves: Description of turbulence *J. Geophys. Res.* **109**, C07015

[2] Brocchini, M. 2013 A reasoned overview on Boussinesq-type models: the interplay between physics,mathematics and numerics. *Proc. R. Soc.* **469**

[3] Delis, A.I., Nikolos, I.K. & Kazolea, M. 2010. Performance and comparizon of cell-centered and node centered unstructured finite volume discretizations for shallow water free surface flows. *Archives of computational methods in engineering (ARCME)*, **18**, 57-118.

[4] Demirbilek, Z., Zundel, A. & Nwogu, O. 2005a. BOUSS-2D wave model in the SMS: I. Graphical interface. Coastal and Hydraulics Laboratory Technical Note CHETNI- 69. Vicksburg, *MS: U.S. Army Engineer Research and Development Center.*

[5] Demirbilek, Z., Zundel, A. & Nwogu, O. 2007. Boussinesq Modeling of Wave Propagation and Runup over Fringing Coral Reefs, Model Evaluation Report. Coastal and Hydraulics Laboratory Technical Note CHLTR0712. Vicksburg, *MS: U.S. Army Engineer Research and Development Center.*

[6] Fedotova Z.I., Khakimzyanov G.S. & Dutykh, D. 2014. Energy equation for certain approximate models of long-wave hydrodynamics. *Russ. J. Numer. Anal. Math. Modelling***29(3)**, 167–178.

[7] Filippini, A., Kazolea, M. & Ricchiuto, M. 2015. A flexible genuinely nonlinear approach for nonlinear wave propagation, breaking and runup. *Paper submitted to J. Comp. Phys.*

[8] Habin, G., Yanabao, L., Shaowu, L., & Luwen., Q. 1993. Application of a Boussinesq wave model. *Internation Conference of Estuaries and Coasts*, **2003**, China.

[9] Kazolea, M. & Delis, A.I. 2013. A well-balanced shock capturing hybrid finite volume -finite difference numerical scheme for extended 1D Boussinesq models. *Applied Numerical Mathematics*, **67**, 167–186.

[10] Kazolea, M. , Delis, A.I. & Synolakis C.E 2014. Numerical treatment of wave-breaking on unstructured finite volume approximations for extended Boussinesq-type equations *Journal of Computational Physics*, **271** , 281–305.

[11] Kennedy, A.B., Kirby, J.T.,. & Dalrymple R.A 2000. Boussinesq modeling of wave transformation, breaking and runup. Part I: 1D *J. Waterw. PortCoast. OceanEng*, **126** , 39–47.

[12] Lannes, D. 2013. The water waves Problem. Mathematical Analysis and Asymptotics *American Mathematical Society, Mathematical surveys and monographs*, **188**

[13] Madsen, P.A., Sorensen, O.R. & Schaffer, H.A 1997. Surf zone dynamics simulated by a Boussinesq type model, Part II. Surf beat and swash oscillations for wave groups and irregular waves. *Coastal Eng.*, **32**, 289–319.

[14] Mase, H. 1995. Frequency down-shift of swash oscillations compared to incident waves. *J. Hydr. Res.*, **33**, 397–411.

[15] Nwogu, O. 1993. An alternative form of the Boussinesq equations for nearshore wave propagation. *Jouranl of Waterway, Port, Coastal, and Ocsean Engineering*, **119**, 618–638.

[16] Nwogu, O. 1996. Numerical prediction of breaking waves and currents with a boussinesq model. *Proceedings 25th International Conference on Coastal Engineering.*, **4:4**, 807-4–820.

[17] Roeber, V., Cheung, K.F. & Kobayashi, M.H. 2010. Shock-capturing Boussinesq-type model for nearshore wave processes. *Coastal Engineering*, **57**, 407–423.

[18] Tonelli, M. & Petti, M. 2012. Shock-capturing Boussinesq-type model for irregular wave propagation *Coastal Engineering*, **61**, 8–19.

[19] Wei, G., Kirby, J.T 1995. A time-depented numerical code for extended Boussinesq equations. *Jouranl of Waterway, Port, Coastal, and Ocsean Engineering*, **120**, 251–261.

[20] Wei, G., Kirby, J.T & Sinha, A. 1999. Generation of waves in Boussinesq models using a source function approach. *Coast. Eng.*, **36**, 271.

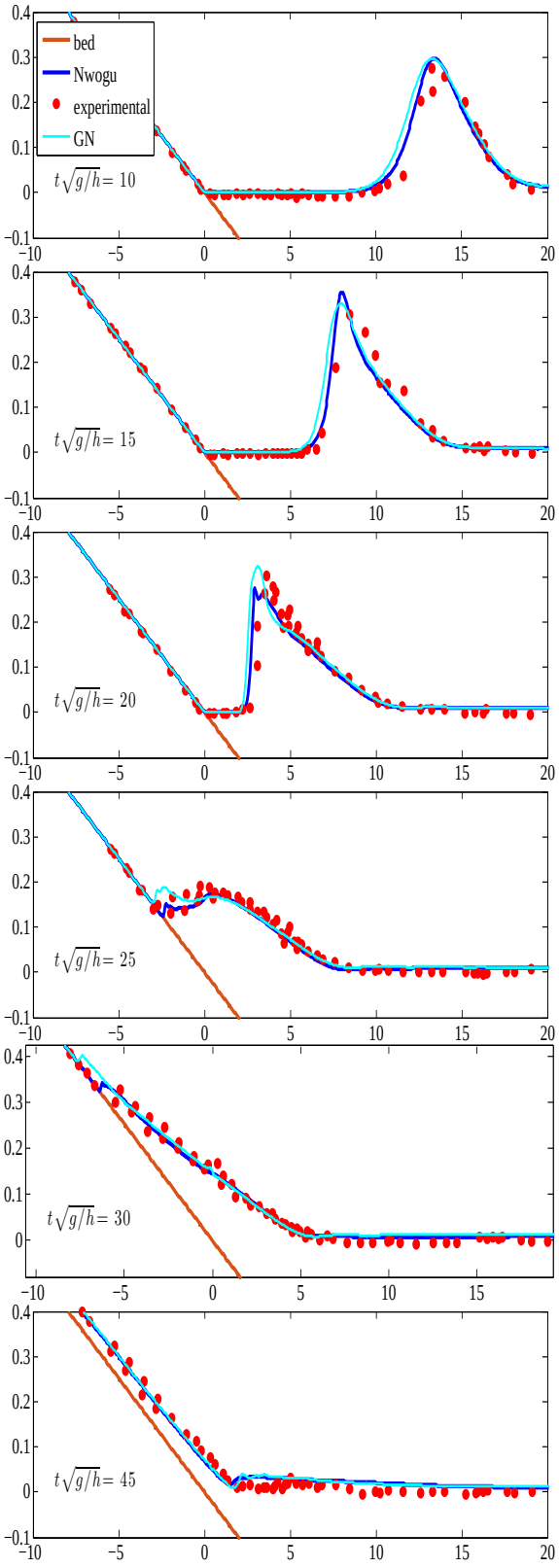

Figure 2: Free surface elevation of solitary wave run-up on a plane beach.

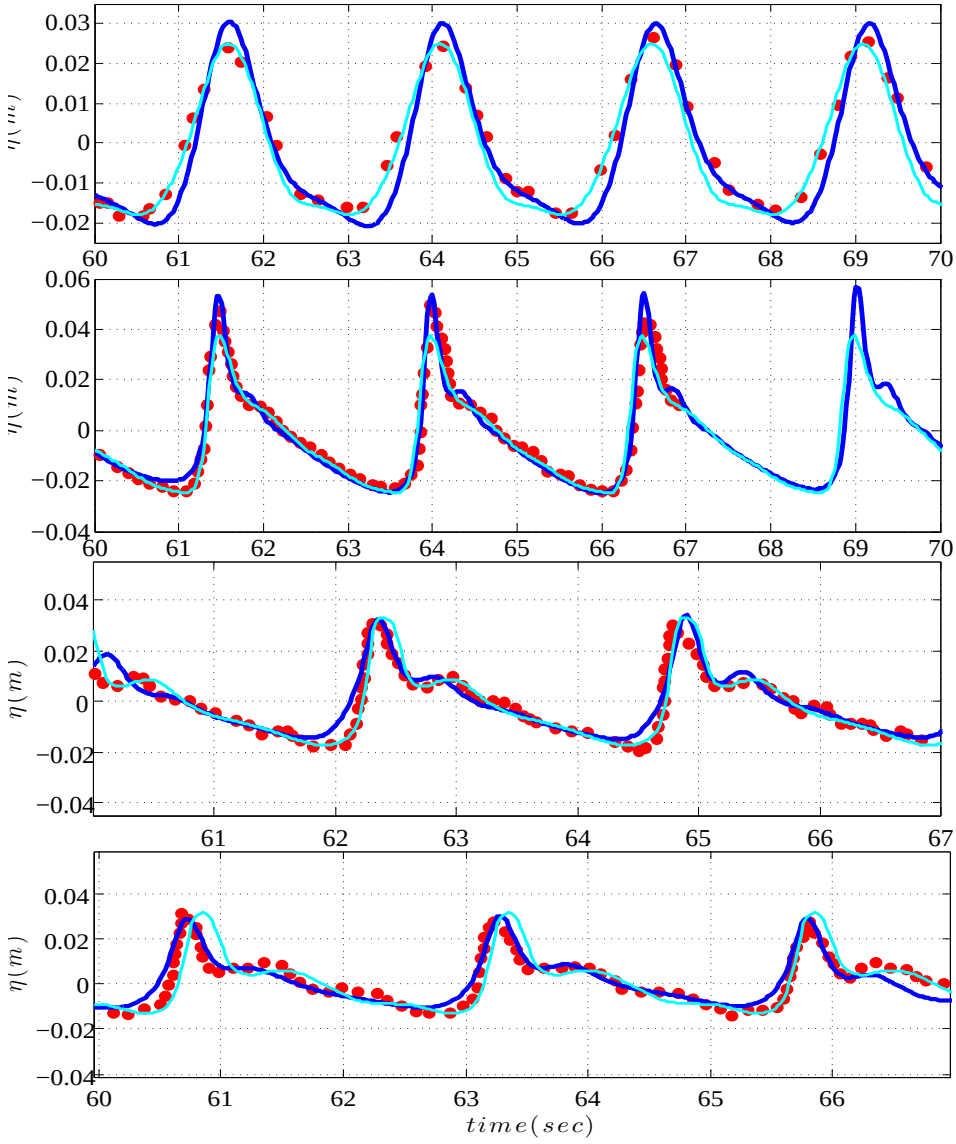

Figure 3: Time series of surface elevation at wave gauges for Nowgu's eq. (blue) and GN eq. (cyan)

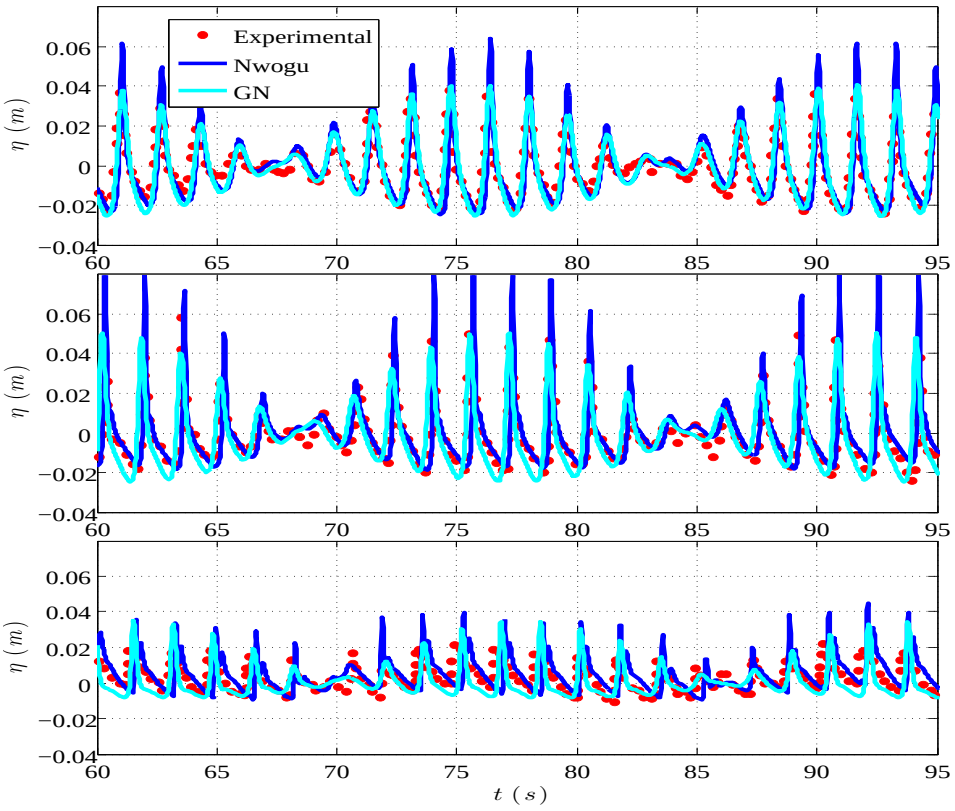

Figure 4: Time series of surface elevation at wave gauges for test case B.

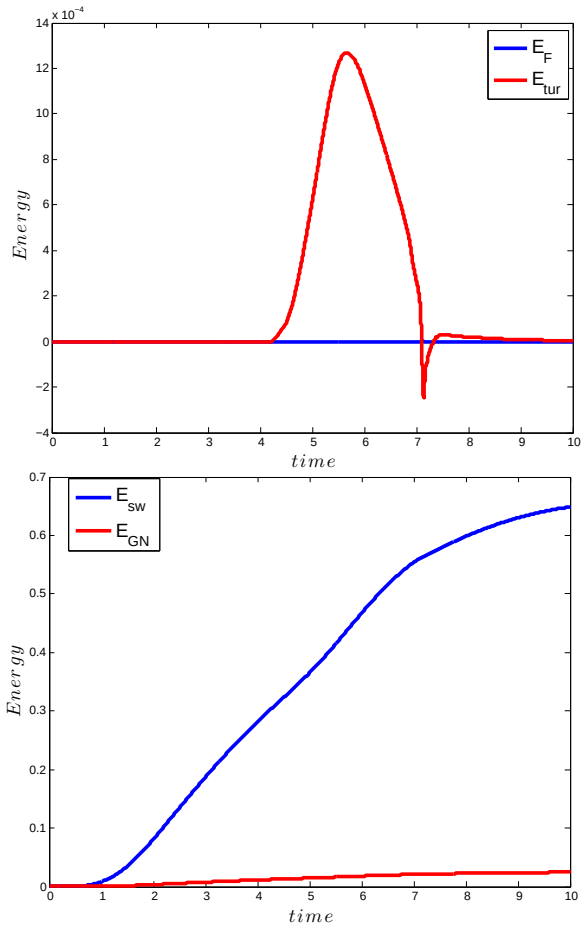

Figure 5: Solitary wave over a slope, using Nwogu's equations

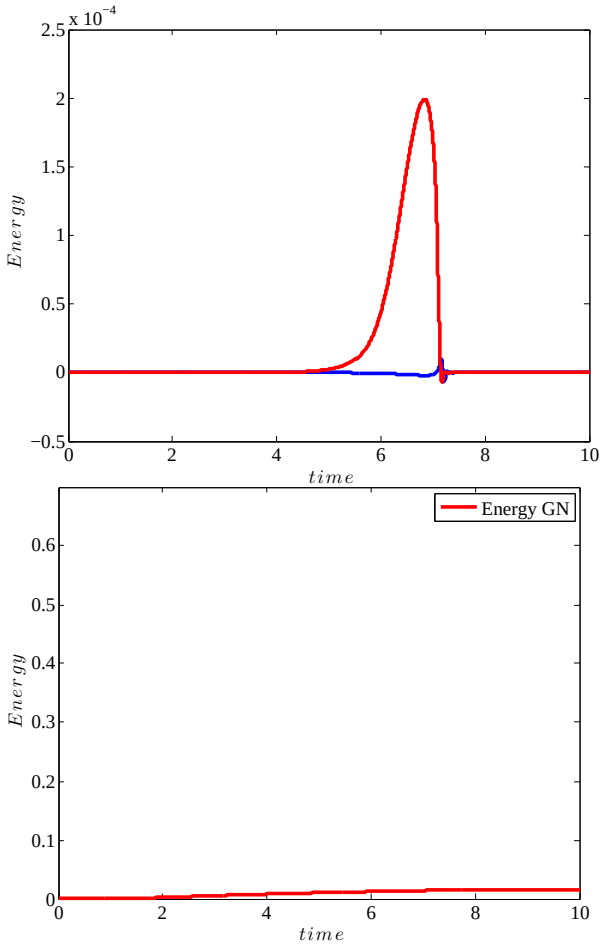

Figure 6: Solitary wave over a slope, using GN's equations

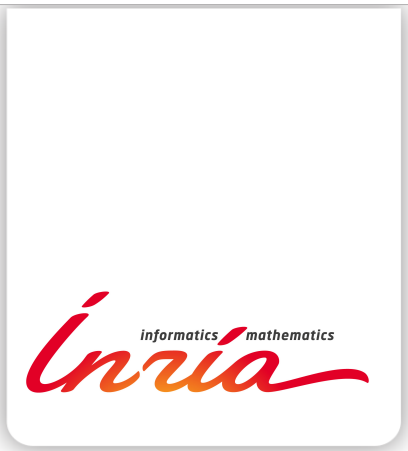

RESEARCH CENTRE
BORDEAUX – SUD-OUEST

351, Cours de la Libération
Bâtiment A 29
33405 Talence Cedex

Publisher
Inria
Domaine de Voluceau - Rocquencourt
BP 105 - 78153 Le Chesnay Cedex
inria.fr

ISSN 0249-6399